Open
Published Online: 31 December 2013
Accepted: December 2013

Performance optimization of apodized FBG-based temperature sensors in single and quasi-distributed DWDM systems with new and different apodization profiles

AIP Advances **3**, 122125 (2013); https://doi.org/10.1063/1.4859115

Nazmi A. Mohammed[1], Taha A. Ali[2, a)], *and* Moustafa H. Aly[2, b)]

View Affiliations

ABSTRACT

In this work, different FBG temperature sensors are designed and evaluated with various apodization profiles. Evaluation is done under a wide range of controlling design parameters like sensor length and refractive index modulation amplitude, targeting a

such as apodization window roll-off rate, asymptotic sidelobe (SL) decay level, number of SLs, and average SL level (SLav). Evaluation techniques like reflectivity, Full width at Half Maximum (FWHM), and Sidelobe Suppression Ratio (SLSR) are also used. A "*New*" apodization function is proposed, which achieves better performance like asymptotic decay of 18.4 dB/nm, high SLSR of 60 dB, high channel isolation of 57.9 dB, and narrow FWHM less than 0.15 nm. For a single accurate temperature sensor measurement in extensive noisy environment, optimum results are obtained by the Nuttall apodization profile and the new apodization function, which have remarkable SLSR. For a quasi-distributed FBG temperature sensor the Barthann and the new apodization profiles obtain optimum results. Barthann achieves a high asymptotic decay of 40 dB/nm, a narrow FWHM (less than 25 GHZ), a very low SLav of −45.3 dB, high isolation of 44.6 dB, and a high SLSR of 35 dB. The new apodization function achieves narrow FWHM of 0.177 nm, very low SL of −60.1, very low SLav of −63.6 dB, and very high SLSR of −57.7 dB. A study is performed on including an unapodized sensor among apodized sensors in a quasi-distributed sensing system. Finally, an isolation examination is performed on all the discussed apodizations and a linear relation between temperature and the Bragg wavelength shift is observed experimentally and matched with the simulated results.

I. INTRODUCTION

The invention of the fiber Bragg grating (FBG) was nominated as one of the milestone events in the history of optical communications, ranking even with the invention of the Laser.[1] FBGs have become an essential optical telecommunication component as fiber laser reflectors, wavelength division multiplexing (WDM) devices, gain flattening devices and dispersion compensator elements.[2] FBGs exhibit well-behaved wavelength responses to temperature and strain, which can be exploited for accurate wavelength tuning and the development of sensor transducer-element.[3] In the area of sensing applications, FBG is used as temperature,[4–7] strain,[6,8] pressure,[9] displacement,[10] humidity,[11] acceleration,[12] high magnetic field,[13] force,[14] medical,[7,15] acoustic,[16] and chemical[17] sensor elements.

Quite several important characteristics make FBG sensors attractive for sensing applications. FBG sensors are intra-core fiber element and are wavelength encoded, eliminating the amplitude or intensity variation problem existing in many other fiber sensors types.[18] The wavelength-encoded nature facilitates WDM by assigning individual sensors to a different slice of the available source spectrum.[19]

FBG temperature sensor is one of the main examples of FBG-based sensors clearly

sensors over other techniques is the ability to multiplex several FBGs into single fiber for long-range quasi-distributed sensing. Not to mention, the ease with which spectral information can be demultiplexed allows the value of each FBG temperature sensor to be extracted as a function of position along the length of the fiber.[20] Distributed sensors are particularly attractive for use in applications where monitoring of the temperature is required at a large number of points or continuously over the path of the fiber. Typical examples of applications areas are temperature profiling in electrical power transformers, generators, reactor systems, process control systems and fire detection systems.[21] FBG temperature sensors operate over a wide range of temperature and are ideal for remote measurements. Also, the small size and weight and the great flexibility that allow access to restricted areas made FBG temperature sensors attractive for many applications.[20,21]

For good and efficient temperature sensor, the broad spectral response can result in poor sensitivity and hence should be avoided.[22] High reflectivity, low sidelobes, narrow FWHM and high sensitivity should be obtained. DWDM FBG system designs require narrow passbands (usually 0.4 nm wide), steep roll-off to reject adjacent channels, and stable operation over increased temperature.[23] Some important considerations should be taken into account if distributed sensing is performed:

The center wavelength of each FBG sensor should be unique[24] for each sensor with enough separation to prevent adjacent reflection peaks interference and avoid the undesirable influence that sidelobes might have on FBGs central wavelength measurement accuracy.

It is preferable to space the Bragg wavelengths of different FBGs closely for efficient bandwidth usage. The more the wavelength spacing is, the higher the isolation and the less the number of sensors in the spectral range of the optical source.

Maximum predicted temperature range is one of the major factors that will affect the minimum separation between adjacent sensors in the wavelength domain and hence the number of sensors in the wavelength-range.[24] FWHM is one of the minimum-separation factors.[24] Small FWHM is preferred for accurate measurement, but it will be on the expense (increase) of sensor length. Small sensor length is mandatory when measuring temperature for discrete point.

SLSR is also one of the minimum separation factors, and preferred to be high to avoid the situation that the sidelobes may affect the adjacent sensor reflectivity.[20] Reducing or eliminating the sidelobes will result in higher SNR and avoid the possible confusion of a sidelobe with an FBG peak.

separation range and hence, increase the number of sensors in the spectral range, increase the isolation, and minimize the adjacent sensors interference. With FBG apodization technology, the central wavelength is stable and SLSR is high.[25] The strong apodization provides the dramatic diminution of the sidelobes to obtain sharp and marked spectral edges, which in turn leads to more accurate measurements.[26]

Although apodization technique is used widely in different FBG applications,[27,28] few literature reviews deal with optimizing temperature sensor performance using apodization technique.[20,22,29,30]

In this work, we demonstrate the effect of different apodization profiles (Uniform, Gaussian, Hamming, Barthann, New apodization function, and Nuttall) on temperature sensor FBG-based. Reasons for choosing those apodization functions are due to their distinctive qualities. The Uniform profile has high reflectivity pattern, small FWHM, and it will be a reference to compare with other apodization profiles. The Gaussian profile, which is a typical apodization function, has a narrow FWHM beside the high reflectivity pattern and its low sidelobes. The Hamming profile has high reflectivity, high SLSR, and small FWHM. The Barthann profile has a good behavior for the roll-off rate, and asymptotic decay in addition to a good reflectivity. Finally, the Nuttall profile which has very low sidelobes, extremely low average sidelobes, and remarkable high SLSR.

Design parameters (length, L, and refractive index modulation amplitude,Δn_{ac}) will be optimized to achieve a remarkable sensing performance for single and quasi-distributed temperature sensing system suitable for DWDM sensing systems. To meet this optimization, new performance evaluation techniques are used together with previous literature review techniques to optimize the performance of FBG temperature sensor suitable for single and quasi-distributed temperature sensing system. Number of sidelobes, sidelobes decay level, apodization functions roll-off rate, sidelobes analysis (sidelobe strength, sidelobe average, and SLSR), reflectivity, FWHM, and the effect of changing FBG length and refractive index modulation amplitude on the previous performance evaluation parameters are used.

After optimizing the FBG-based temperature sensor, sensor linearity will be tested. A simulation is used to show the effect of including uniform FBG temperature sensor among apodized sensors in DWDM quasi-distributed temperature sensing system. Finally, an isolation examination is performed on all the discussed apodizations.

This paper is organized as follows: Section II is the theory and modeling. Section III represents the results and discussion that evaluate FBG-based temperature sensor with

profile, and Nuttall) under wide range of L and Δn_{ac} using several old and new evaluation techniques to achieve remarkable performance for single and quasi-distributed sensing systems and shows the matches between the experimental and simulated results. Section IV summarizes in a comparison the evaluation techniques discussed in sec. III and presents the optimized choice for single FBG temperature sensor. Section IV discusses the optimum choice for quasi-distributed sensing system apodization profile with the optimized parameters, effect of including a different apodization with the optimized apodization profile, effect of temperature change on the quasi-distributed sensing system, effect of the discussed apodizations on the adjacent channels isolation, and a linearity check with a comparison with experimental results. Sec. VI concludes the obtained results.

II. THEORY AND MODELING

A. Apodization and reflectivity

A periodic refractive index variation in the core of an optical fiber will exhibit specific reflections at the Bragg condition:

$$\lambda_b = 2n_{eff}\Lambda \tag{1}$$

Where λ_b is wavelength of the peak reflection amplitude (Bragg grating wavelength), n_{eff} is the effective refractive index of the guided mode, and Λ the grating period. In our model, the coupled-mode theory (CMT) is used to describe the behavior of the Bragg gratings.

The FBG is completely characterized by its refractive index distribution $n(z)$ along the fiber as shown in Figure 1

$$n(z) = n_0 + A(z)\Delta n_{ac}(z)\cos((2\pi/\Lambda)z + \theta(z)) + \Delta n_{dc}(z) \tag{2}$$

where z is the position, n_0 is the refractive index prior to grating inscription, $A(z)$ is the apodization function, Δn_{ac} is the refractive index modulation amplitude, Λ is the design grating period, θ is the period chirp, Δn_{dc} is the average change in refractive index.

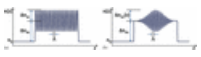

FIG. 1. (a) Homogeneous FBG refractive index Profile, (b) Apodized FBG index Profile.

Using CMT, the reflectivity of the grating with constant modulation amplitude and period is given by:[18]

$$R(l,\lambda) = k^2 sinh^2(sl)/\left(\Delta\beta^2 sinh^2(sl) + s^2 cosh^2(sl)\right) \quad (3)$$

Where $R(l, \lambda)$ is the reflectivity, k is the coupling coefficient, $\Delta\beta = \beta - \pi/\Lambda$ is the detuning wavevector, $\beta = 2\pi n_0/\lambda$ is the propagation constant and finally $s^2 = k^2 k2 - \Delta\beta^2$.

Homogenous gratings have uniform Δn_{ac} and Δn_{dc} with constant Λ (Figure 1). Sidelobes come from the abrupt strong index step at both input and output of the grating.

Apodized gratings have variations along the fiber in the refractive index modulation envelope (Δn_{ac}) with constant period (Λ) and constant DC refractive index function (Δn_{dc}) as shown in Figure 1.

B. Coupled mode theory (CMT) and T-matrix method (TMM)

Coupled Mode Theory (CMT) describes the behavior of Bragg grating, where the counter-propagating fields inside the grating structure are related by coupled differential equations. Transfer Matrix Method (TMM) will be used to solve coupled mode equations for Bragg grating structure to obtain its spectral response. The T-matrix relates the input and output of the Bragg grating and is ideal for analyzing a cascade of gratings. More details about CMT and TMM are found in reference.[18]

C. Temperature sensitivity of FBG

The Bragg wavelength depends on the effective index of refraction of the core and the periodicity of the grating and both of them will be affected by changes in temperature.[18]

$$\Delta\lambda_b = \lambda_b (\alpha_{\Lambda+}\alpha_n)\Delta T \quad (4)$$

Where $\alpha_\Lambda = (1/\Lambda)(\delta\Lambda/\delta T)$ is the thermal expansion coefficient for the fiber (about 0.55×10^{-6} for silica), and $\alpha_n = (1/n)(\delta n/\delta T)$ is the thermo-optic coefficient (approximately 8.6×10^{-6} for a germanium-doped, silica-core fiber). Clearly, the index change is by far the dominant effect. The expected sensitivity for 1550 nm Bragg grating is approximately $14 pm/°C$.[18]

The following apodization profiles will be used in this work to design an FBG-based temperature sensor:

1. Uniform

$$A(x) = 1 \quad 0 \le x \le L$$

2. Gaussian Function

$$A(x) = exp\left(-ln2(2(x - L/2)/0.5L)^2\right) \quad 0 \le x \le L$$

3. Hamming Function

$$A(x) = 0.54 - 0.46\cos(2\pi x/L) \quad 0 \le x \le L$$

4. Barthann Function

$$A(x) = 0.62 - 0.48\,\mathbf{abs}\,(\mathbf{x}/L - 0.5) + 0.38\cos(2\pi(x/L - 0.5)) \quad 0 \le x \le L$$

5. New Function

$$A(x) = \cos^8(2x/L - 1)$$

6. Nuttall function

$$A(x) = a_0 - a_1\cos(2pi(x/L)) + a_2\cos(4pi(X/L)) - a_3\cos(6pi(x/L)) \quad ($$

Where

$$a_0 = 0.3635819 \quad a_1 = 0.48917755$$
$$a_2 = 0.1365995 \quad a_3 = 0.0106411$$

III. RESULTS AND DISCUSSION

A. Introduction

Based on the described model, the simulations are performed for step index, single mode fiber with 2 μm core radius. Bragg wavelength is set to 1550 nm. Δn_{ac} varies from 0.01×10^{-4}

simulations are repeated with varying L from 1000 to 19000 μm while Δn_{ac} is maintained at 4×10^{-4}. These values are chosen to meet previous literature reviews.[3,20,31–33]

Table I is the apodization functions' specifications. The Rectangular window has the highest magnitude and the lowest mainlobe width but with high leakage factor and low relative low sidelobe attenuation. The Gaussian window has the narrowest mainlobe width among the apodized profiles (not including Rectangular window) with high magnitude. The Hamming window has the highest magnitude among the apodization functions. The Barthann window has the highest roll-off rate with high magnitude. The New apodization function has the lowest leakage factor and very high relative sidelobe attenuation. Nuttall has the lowest sidelobe attenuation, lowest leakage factor, and highest relative sidelobe attenuation.

Table I.

Window functions properties.

	Roll-off Rate (dB/Octave)	Magnitude (*dB*)	Leakage factor	Relative sidelobe attenuation (*dB*)	Mainlobe width (−*3dB*)
Rectangular	4.1	40	9.26%	−13.3	0.015625
Gaussian	4	34.3	0.04%	−37.2	0.025391
Hamming	4	34.7	0.03%	−42.6	0.025391
Barthann	8.2 to 11	34	0.03%	−35.9	0.027344
New	4.1	32.7	0%	−61.2	0.03125
Nuttall	2.6	31.3	0%	−95.8	0.035156

Fig. 2(a-a′) and 2(b) show different apodization functions that are depicted in frequency domain and time domain respectively. Concerning the FWHM, the Gaussian has the narrowest value and the Nuttall has the widest among the apodization functions. For sidelobe suppression ratio (SLSR), the Nuttall apodization function has the highest SLSR

rate, the Barthann function has a better roll-off rate than other apodization functions with 8.2 dB/octave. These windows' specifications will be applied on the FBG temperature sensor and evaluated in the following sections.

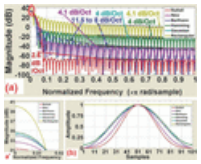

FIG. 2. Apodization function in (a-a′) frequency and (b) time domain.

PPT | High-resolution

B. Performance evaluation based on number of sidelobes and decay level

In this section, the apodization functions (windows) mentioned and discussed in sec. II D and III A, will be applied to the FBG reflectivity pattern to evaluate their impact on the FBG reflectivity pattern specifications (Reflectivity peak, FWHM, sidelobes asymptotic decay, and number of sidelobes behavior). Evaluation is done under different values of L and Δn_{ac} within the range of 2 nm as shown in Fig. 3. This way of presentation is a point of view that will be used to verify results presented separately for each evaluation parameter.

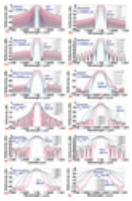

FIG. 3. FBG Reflectivity curves. At L = 10 mm (a) Uniform FBG,(b) Gaussian FBG,(c) Hamming FBG, (d) Barthann FBG, (e) The New apodization function, and (f) Nuttall FBG. At $\Delta n_{ac} = 4 \times 10^{-4}$ (g) Uniform FBG, (h) Gaussian FBG, (i) Hamming FBG, (j) Barthann FBG, (k) the New apodization function and (l) Nuttall FBG.

PPT | High-resolution

PDF

The unique importance of this section is that it will discuss two new evaluation parameters: number of sidelobes and the asymptotic decay level under the same range of L and Δn_{ac} (cannot be carried or viewed in sections III C and III D).

Fig. 3(a)–3(f) displays the reflectivity versus wavelength for Uniform, Gaussian, Hamming, Barthann, New, and Nuttall apodized FBG respectively, at constant length L = 10000 μm and various Δn_{ac} (0.5×10^{-4}, 1×10^{-4}, 2×10^{-4}, 4×10^{-4} and 5×10^{-4}).

Fig. 3(g)–3(l) are the reflectivity versus wavelength for Uniform, Gaussian, Hamming, Barthann, New, and Nuttall apodized FBG respectively, at constant $\Delta n_{ac} = 4 \times 10^{-4}$ and various L (2000, 3000, 4000, 5000 and 9000 μm).

From the previous discussion, one can say:

- The higher the Δn_{ac}, the wider the FWHM and the more the reflectivity for fixed value of length. Number of sidelobes is almost the same (within each apodization function and within the uniform profile) with increasing Δn_{ac}. In addition, for apodized profiles a lower reflectivity with lower sidelobe level is observed compared to uniform one.
- The longer the grating, the narrower the FWHM and the more the reflectivity for fixed value of Δn_{ac}. Up to about 5 mm, a small variation in length induces a great variation in FWHM; this will be verified again in sec. III D 2 using the FWHM curve. Number of sidelobes increases with the grating length for both uniform and apodized FBG. Again, for apodized FBG, a lower reflectivity with lower sidelobe level is observed compared to uniform one.

Comparing the uniform FBG spectrum (Fig. 3(a) and 3(g) with the apodized FBG (Fig. 3(b)–3(f) and 3(h)–3(l), one observes a high suppression of sidelobes in reflectivity curve (for apodized FBG) ranging from about 35 up to more than 100 dB at the cost of reduced reflected power. Keeping in mind that, the reflected power can be increased by increasing the length of the grating.[34]

By observing the sidelobe asymptotic decay (within range of 2 nm), for the uniform and apodized gratings, one finds that: for uniform grating sidelobes (Fig. 3(a) & 3(g)), the asymptotic decay is about 18.8 dB/nm and in Gaussian Fig. 3(b) & 3(h) it ranges from 12 to 13 dB/nm. Hamming function Fig. 3(c) & 3(i) has sidelobes asymptotic decay of about 5 dB/nm. Barthann function Fig. 3(d) & 3(j) has sidelobes asymptotic decay of about 40 dB/nm. New apodization function Fig. 3(e) &3(k) has sidelobes asymptotic decay ranging from 13.3 to 18.4. Nuttall function Fig. 3(f) & 3(l) has an asymptotic decay from 4.25 to 10 dB/nm. These results

Barthann has the highest roll-off rate.

C. Performance evaluation using reflectivity, FWHM and sidelobes analysis under constant sensor length

In this section, the uniform and apodized FBG is tested seeking optimum performance parameters for a remarkable FBG temperature sensor performance. This performance evaluation is carried in the range of Δn_{ac} (from 0.01×10^{-4} to 14.4×10^{-4}) with constant length L (10000 μm).

1. Reflectivity

In Fig. 4, it is shown that, the Nuttall profile has the lowest reflectivity, whereas the Hamming one provides the highest value among the simulated apodized profiles. The apodization process reduces the reflectivity, compared to the uniform FBG (matched with the result obtained in sec. III A and III B). It is observed that, the reflectivity increases with Δn_{ac}. Reflectivity increases rabidly up to about $\Delta n_{ac} = 2 \times 10^{-4}$ and reaches saturation at Δn_{ac} of 3×10^{-4} for Uniform FBG, 5×10^{-4} for Gaussian, Hamming, Barthann, and Nuttall apodized FBG, and 6×10^{-4} for New Apodized FBG.

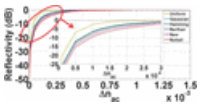

FIG. 4. FBG reflectivity at constant value of L for uniform and different apodization profiles.

2. FWHM

Fig. 5 displays the FWHM for uniform and apodized FBG required to design an optimum performance temperature sensor at different values of Δn_{ac}. Like reflectivity, the FWHM increases with Δn_{ac}. The reason behind representing the FWHM across five figures is that the FWHM for the uniform and apodized FBG changes its behavior along the mentioned range of Δn_{ac}.

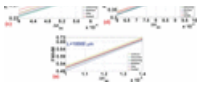

FIG. 5. FWHM (nm) versus the change in Δn_{ac} (a) range from 0.01 × 10⁻⁴to 2×10⁻⁴ (b) range from 2 × 10⁻⁴ to 4 × 10⁻⁴ (c) range from 4 × 10⁻⁴ to 6.1 × 10⁻⁴ (d) range from 6 × 10⁻⁴ to 10 × 10⁻⁴ (e) range from 1 × 10⁻³ to 1.4 × 10⁻³

In Fig. 5(a), in the range from 0.01 × 10⁻⁴ to 2 × 10⁻⁴, the Nuttall profile has the highest bandwidth, and Both Gaussian and Hamming provides the lowest bandwidth among the apodization function but still is higher than the FWHM of the uniform FBG (The Hamming and Gaussian curves are almost the same). This means that, in this range, all apodization functions are broadening the FBG temperature sensor spectrum. In addition, all the apodization profiles are still under an FWHM of 0.2 nm (suitable for DWDM systems).

In Fig. 5(b), in the range from 2 × 10⁻⁴to 4 × 10⁻⁴, the Nuttall profile has the highest bandwidth, and the Gaussian provides the lowest bandwidth even less than the uniform one. In this range, all apodization functions are broadening the FBG temperature sensor spectrum except the Gaussian function.

In Fig. 5(c), the range from 4 × 10⁻⁴ to 6.1 × 10⁻⁴, the Nuttall profile has the highest bandwidth (similar to the two previous ranges), and the Gaussian function provides the lowest bandwidth with less FWHM than the uniform one. Different from previous case, one notes that, in this range, the New apodization function provides a lower bandwidth than the uniform one. Nuttall is the only one that broadens the FBG temperature sensor spectrum in this range.

In Fig. 5(d) & e, the range from 6 × 10⁻⁴to 10 × 10⁻⁴ and 1 × 10⁻³ to 1.4 × 10⁻³ respectively, the uniform one has the highest FWHM and all other apodization functions provides less bandwidth where the Barthann function provides the lowest FWHM.

3. Sidelobe analysis

A common way to improve the bandwidth usage, the adjacent channels isolation and the crosstalk of quasi-distributed FBG temperature system, is to reduce the near-in sidelobes. Sidelobes are wasted energy. Although reduction in the sidelobe strength is a target, one cannot ignore that it will be on the expense of the reflectivity and FWHM. One can achieve a significant reduction on the near-in sidelobe strength (maximum sidelobe), but with also

sidelobe strength is not enough. One should combine the maximum sidelobe reduction with its effect on reflectivity (mainlobe) reduction, in other words SLSR. Thus, both sidelobe strength and SLSR are important FBG temperature sensor design parameters. Nevertheless, SLSR is not enough to characterize the FBG temperature-sensor performance parameters concerning sidelobes. Maximum sidelobe strength or even the SLSR does not predict or show the average wasted energy. Reducing the average sidelobe means increasing reflectivity (mainlobe). It is desirable to estimate the average sidelobe level of an FBG sensor, and to know which reflection pattern is reasonable to choose the suitable design parameters. For the entire previous discussion, detailed sidelobe analysis will be presented in the following sections.

A. Maximum sidelobe strength.

In Fig. 6(a), the maximum sidelobe is shown as a function of $\Delta n_{ac}$for uniform and various FBG apodization profiles required to design optimum FBG temperature sensor. It is clear that the, the Gaussian, Hamming, and Barthann apodization profiles have the maximum SLs but less than the uniform one with more than 20 to 40 dB. The New apodization function achieved lower SLs than the Uniform one by more than 50 dB. The Nuttall apodization profile achieved the lowest sidelobe strength over the entire range of Δn_{ac} (with more than 80 dB lower than the Uniform one). To the best of our knowledge, it is the lowest FBG temperature sensor sidelobe strength for an apodization function.

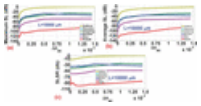

FIG. 6. Sidelobes Analysis (a) Maximum Sidelobe Strength, (b) Average Sidelobe, (c) SLSR.

B. Average sidelobe.

In Fig. 6(b), and again to our knowledge, it is the first time for an FBG temperature sensor that the average sidelobe is to be discussed and depicted. The average sidelobes as function of Δn_{ac} is depicted. It is shown that, the Gaussian and Hamming apodization profiles have the maximum sidelobe average (maximum wasted energy) but less than the uniform one.

of Δn_{ac}. Nuttall apodization function provides an average sidelobe level of −128 dB at Δn_{ac} = $0.1 \times 10^{-4}$with a reflectivity of 0.12%, maximum sidelobe of −125.5 dB and an FWHM of 0.1545 nm. To avoid bandwidth broadening, the range of $\Delta n_{ac} = 7 \times 10^{-4}$ to 14.4×10^{-4} is to be used. This range has less FWHM than the uniform one and an average sidelobe of −92 dB at Δn_{ac} of 10×10^{-4} with a reflectivity of 99.6% and an FWHM of 0.515 nm. These are the optimum values of an FBG temperature sensor average sidelobe.

C. SLSR.

In Fig. 6(c), the SLSR is presented and depicted under the same range of Δn_{ac}. It is clear that, the Gaussian, Hamming, and Barthann apodization functions have the lowest (not good) SLSR but greater than the uniform one. The New apodization function achieves very high SLSR with more than 50 dB difference than the Uniform one. The Nuttall apodization function achieves a remarkable SLSR with a value greater than 85 dB from that of the uniform one over the entire range of Δn_{ac}. This is also an optimum temperature sensor SLSR.

D. Performance evaluation using reflectivity, FWHM and sidelobe analysis under constant refractive index modulation amplitude Δn_{ac}

In this section, the uniform and apodized FBG are evaluated seeking optimal design parameters for a remarkable FBG temperature sensor performance in single and quasi-distributed sensing systems. This performance evaluation is in the range of L = 10000 to 19000 μm with constant $\Delta n_{ac} = 4 \times 10^{-4}$ to study the grating length effect.

1. Reflectivity

In Fig. 7, it is shown that the reflectivity is increasing with the grating length for all profiles. The Nuttall apodization function has the lowest reflectivity and reaches the saturation at 16 mm. The Hamming profile provides the highest reflectivity among the apodization function but still is less than the uniform one, and reaches the saturation at a shorter length of 11 mm. The uniform apodization has the highest reflectivity and reaches about 100% at the shortest length (relative to the apodized profiles) of 7 mm.

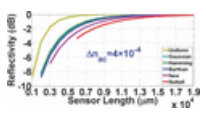

FIG. 7. Verifying FBG reflectivity with the grating length at constant refractive index.

2. FWHM

FWHM performance is getting lower (improved) with the increase of grating length as shown in Fig. 8(a) & 8(b) for both uniform and apodized profiles. The uniform profile has the lowest (best) FWHM value up to the length of 6 mm. The Gaussian apodization profile has the lowest (best) FWHM value among all others from length of 6 mm and above (Fig. 8(b)). All apodization profiles are providing a narrower FWHM than the uniform one when the grating length is from 10 to 16 mm. The Nuttall apodization function has the narrower bandwidth than the uniform one only above 16 mm at $\Delta n_{ac} = 4 \times 10^{-4}$.

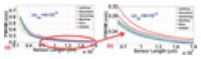

FIG. 8. Verifying FBG FWHM with the grating length at constant refractive index.

For gratings shorter than approximately 5 mm, a small variation in the length induces a great variation in FWHM as shown in Fig. 8. This result agrees with that in sec. III B. On the other hand, gratings longer than 14 mm are almost not affected by length variation.

3. Sidelobe analysis

As mentioned in sec. III C 3 for the importance of SL analysis, we will repeat the investigation of sidelobe effect, but with studying the effect of L on sidelobes at constant Δn_{ac}.

A. Maximum sidelobe.

From Fig. 9(a), the Nuttall apodization function has the lowest and best sidelobe strength over the entire period of length with about 60 dB difference (lower) from the Gaussian apodization function and with more than 90 dB difference (lower) from the uniform profile. The uniform profile has the highest sidelobe strength compared to the apodization profiles. This was obvious in sec. III B when comparing sidelobe strength for the uniform profile with sidelobe strength for apodized profiles.

FIG. 9. Sidelobe analysis @ Constant Δn_{ac} (a) Max Sidelobe Strength, (b) Average Sidelobe, (c) SLSR.

B. Average sidelobe.

In Fig. 9(b), the Nuttall apodization function has the lowest average wasted power which reaches –113.2 dB at an FBG length of 9 mm and $\Delta n_{ac} = 4 \times 10^{-4}$.

C. SLSR.

In Fig. 9(c), the Nuttall apodization function provides a remarkable SLSR over the entire range of Length with a value greater than 85 dB from that of the uniform one (reaches –101 dB at L = 6 mm and $\Delta n_{ac} = 4 \times 10^{-4}$). This is the best temperature sensor SLSR up to the date of writing this paper.

IV. COMPARISON

In this section, the obtained results are summarized with comparisons for the evaluation techniques previously discussed using the best samples. This way of presentation helps designers to choose the optimum performance characteristics for accurate FBG-based temperature sensor according to sensing system needs. The following discussion concentrates on extracting the most suitable (optimum) design parameters and apodization profile required to achieve an optimum single FBG temperature sensor performance. Then, it will be used to decide which apodization profile and which optimum design parameters are most suitable for quasi-distributed temperature sensing system. Table II summarizes sections III B–III D.

Table II.

Sections III B–III D Summary.

	No. of SL	Asymptotic decay dB/nm	Constant Parameter	Δn/L	R (%)	FWHM (nm)	SL (dB)	Slav (dB)	SLSR (dB)
	almost the same			$\Delta n_{ac} = 1 \times 10^{-6}$	0.01%	*0.073*	*-53.67*	*-61.34*	13.26
				$\Delta n_{ac} = 5 \times 10^{-5}$	19.70%	*0.079*	-19.74	-27.39	12.68
		18.8	L=10000μm	$\Delta n_{ac} = 1.3 \times 10^{-4}$	71.49%	*0.109*	-11.70	-19.25	10.24

	number of SLs increase with L increase	18.9	$\Delta n_{ac} = 4 \times 10^{-4}$	$L = 1000\mu m$	13.26%	0.771	-24.44	-24.44	15.67
				$L = 5000\mu m$	**91.57%**	0.286	-8.34	-12.79	7.95
				$L = 9000\mu m$	**99.58%**	0.244	−4.47	−11.01	4.45
				$L = 14000\mu m$	**99.99%**	0.224	−2.41	−10.00	2.41
				$L = 19000\mu m$	**100.00%**	0.215	-1.47	-9.52	1.47
Gaussian	almost the same with Δn_{ac} increase	13.4	$L = 10000\ \mu m$	$\Delta n_{ac} = 5 \times 10^{-5}$	5.96%	*0.111*	*-48.99*	*-54.95*	36.74
				$\Delta n_{ac} = 1.3 \times 10^{-4}$	32.51%	*0.125*	-40.04	*-46.4*	35.17
				$\Delta n_{ac} = 2 \times 10^{-4}$	**57.8%**	*0.145*	-40.63	-44.71	38.25
				$\Delta n_{ac} = 3 \times 10^{-4}$	**81.76%**	*0.183*	-37.47	-41.3	36.6
				$\Delta n_{ac} = 4 \times 10^{-4}$	**92.84%**	0.224	-35.6	-38.97	35.27
	number of SLs increase with L increase	12.2	$\Delta n_{ac} = 4 \times 10^{-4}$	$L = 3000\ \mu m$	28.7%	0.409	−40.85	−40.85	35.43
				$L = 7000\ \mu m$	**78.2%**	0.25	−38	−40.25	36.9
				$L = 12000\ \mu m$	**96.7%**	0.215	−34.5	−38.2	34.35
				$L = 19000\ \mu m$	**99.8%**	0.201	-30	-.36.9	30
Hamming	almost the same with Δn_{ac} increase	5.2	$L = 10000\ \mu m$	$\Delta n_{ac} = 1 \times 10^{-4}$	22.5%	*0.118*	*-48.4*	*-51*	42
				$\Delta n_{ac} = 1.6 \times 10^{-4}$	46%	*0.133*	-44.3	*-47.2*	41
				$\Delta n_{ac} = 1.8 \times 10^{-4}$	**53.2%**	*0.139*	-43.3	*-46.2*	40.6
				$\Delta n_{ac} = 2 \times 10^{-4}$	**60%**	*0.146*	-42.4	*-45.3*	40.2
				$\Delta n_{ac} = 3 \times 10^{-4}$	**83.4%**	*0.185*	-39	-41	38
				$\Delta n_{ac} = 4 \times 10^{-4}$	**93.7%**	0.228	-36.4	-38.6	36.1
	number of SLs increase with L increase	5.5	$\Delta n_{ac} = 4 \times 10^{-4}$	$L = 4000\ \mu m$	45.8%	0.334	−44.4	*-47.3*	41
				$L = 6000\ \mu m$	**71.3%**	0.269	−40.8	−42.2	39.4
				$L = 11000\ \mu m$	**95.8%**	0.223	−35.6	−38	35.4
				$L = 19000\ \mu m$	**99.8%**	0.204	-30.4	-35.8	30.4
Barthann	almost the same with Δn_{ac} increase	**40.5**	$L = 10000\ \mu m$	$\Delta n_{ac} = 1.2 \times 10^{-4}$	26.7%	*0.129*	-42	*-48.7*	36.2
				$\Delta n_{ac} = 2 \times 10^{-4}$	**55%**	*0.152*	-37.6	*-45.3*	35
				$\Delta n_{ac} = 3 \times 10^{-4}$	**79.5%**	*0.189*	-33.7	-43	32.7
	number of SLs increase with L	**39.6**	$\Delta n_{ac} = 4 \times 10^{-4}$	$L = 7000\ \mu m$	**75.8%**	0.259	−43.4	−42	42.2
				$L = 15000\ \mu m$	**98.7%**	0.21	−37.7	*-48*	37.7
				$L = 19000\ \mu m$	**99.7%**	0.201	-35.3	*-46.5*	35.2
New	almost the same with Δn_{ac} increase	18.4	$L = 10000\ \mu m$	$\Delta n_{ac} = 1.2 \times 10^{-4}$	20.7%	*0.143*	-67.2	*-69.7*	**60.3**
				$\Delta n_{ac} = 2 \times 10^{-4}$	45.4%	*0.1625*	-62.4	*-65.6*	**59**
				$\Delta n_{ac} = 2.5 \times 10^{-4}$	**59.5%**	*0.1775*	-60.1	*-63.6*	**57.7**
				Δn_{ac}=4× 10^{-4}	**86%**	0.237	-54.2	*-58.8*	**53.5**
	number of SLs increase with L	13.3	$\Delta n_{ac} = 4 \times 10^{-4}$	$L = 6000\ \mu m$	**56.8%**	0.292	−60.5	*-63*	**58**
				$L = 8000\ \mu m$	**74.6%**	0.255	−57.2	*-60.4*	**56**
				$L = 19000\ \mu m$	**99.2%**	0.208	-52.8	*-57.4*	**52.8**
Nuttall	almost the same with Δn_{ac} increase	4.25	$L = 10000\ \mu m$	$\Delta n_{ac} = 1 \times 10^{-6}$	0.001%	*0.1545*	*-120.2*	*-124.76*	**71.01**
				$\Delta n_{ac} = 5 \times 10^{-5}$	2.95%	*0.1565*	*-104.33*	*-118.53*	**89.02**
				$\Delta n_{ac} = 2 \times 10^{-4}$	36.04%	*0.1815*	*-104.07*	*-111.68*	**99.64**
				$\Delta n_{ac} = 2.6 \times 10^{-4}$	**51.43%**	*0.1985*	*-100.94*	*-121.74*	**98.05**
				$\Delta n_{ac} = 3 \times 10^{-4}$	**60.54%**	0.2120	*-100.55*	*-109.86*	**98.37**
				$\Delta n_{ac} = 4 \times 10^{-4}$	**77.90%**	0.2500	*-96.34*	*-107.23*	**95.26**
				$\Delta n_{ac} = 5 \times 10^{-4}$	**88.28%**	0.2915	*-96.09*	*-107.45*	**95.55**
	number of SLs increase with L increase	10	$\Delta n_{ac} = 4 \times 10^{-4}$	$L = 6000\ \mu m$	46.48%	0.3215	*-104.33*	*-106.87*	**101.00**
				$L = 9000\ \mu m$	**71.89%**	0.2605	*-98.27*	*-113.25*	**96.84**
				$L = 12000\ \mu m$	**86.65%**	0.2360	−93.87	*-102.96*	**93.25**
				$L = 14000\ \mu m$	**92.11%**	0.2265	−92.25	*-96.20*	**91.89**
				$L = 19000\ \mu m$	**97.97%**	0.2135	*-89.71*	*-90.79*	**89.62**

Thresholds for reflectivity, FWHM, sidelobe strength (maximum sidelobe), asymptotic decay, average sidelobes, and SLSR are chosen for an FBG-based temperature sensor seeking high measurement performance as follows:

- High reflectivity with more than or equal to 50%
- Narrow FWHM with less than or equal to 0.2 nm (0.4 nm (50 GHZ) is acceptable, suitable for DWDM systems according to ITU standard).
- Sidelobe strength (maximum sidelobe) with less than or equal to −45 dB
- High Asymptotic decay with more than or equal to 30 dB/nm
- Average sidelobe with less than or equal to −45 dB

SLSR with more than or equal to 45 dB

The previous thresholds are suggested with the aid of several sources, vendors and other literature reviews.[35–39]

In Table II, colors are used to help determining the most suitable (optimum) design parameters and apodization profile (based on previously mentioned thresholds) to obtain optimum FBG temperature sensor measurement according to the application needs. “Bold Font” means that this parameter is preferred to be of a high value and “*Italic Font*” means that this parameter is preferred to be of a low value, for optimum FBG temperature sensor.

Table III shows the apodization profiles evaluation summary. Table II and Table III make it clear and easy to designers to select the most suitable design parameters for single and quasi-distributed FBG-based temperature sensor for optimum measurement.

Table III.

Apodization profiles evaluation summary.

	Reflectivity	**FWHM**	**Asymptotic Decay**	**Max S.L.**	**Average S.L.**	**SLSR**
Uniform	Excellent	Very Good	Not Good	Not Good	Not Good	Not Good
Gaussian	Good	Excellent	Good	Good	Good	Good
Hamming	Good	Good	Not Good	Good	Good	Good
Barthann	Good	Excellent	Excellent	Good	Good	Good
New	Good	Good	Good	Very Good	Very Good	Very Good
Nuttall	Good	Good	Not Good	Excellent	Excellent	Excellent

to design a single FBG-based temperature sensor with high reflectivity, narrow bandwidth and to have a good degree of low sidelobes. The Nuttall and the "New" apodization profiles would give very distinctive results. However, it would not be the optimum solution. As in case of free noise single sensing system, Hamming function shows more than adequate performance for sidelobe suppression. The Hamming apodization function with a length of 10000 μm and $\Delta n_{ac} = 3 \times 10^{-4}$ gets high reflectivity of 83.4%, narrow FWHM of 0.185 nm, maximum sidelobes of −39 dB, average sidelobes wasted power of −41 dB, and SLSR of 38 dB (*as marked with single underlined values in* Table II).

Although fiber optics are immune to RFI (radio frequency interference) and EMI (Electromagnetic Interference) noise sources, there exists other sources of noise that may potentially corrupt the data signal from the temperature sensor.[40] An example for an extensive noise environment that can affect the performance of a temperature sensor is the "Radioluminescence" (RL). The luminescence effect may strongly reduce the SNR of the detection system. The luminescence mainly depends on the dose rate and is likely to fluctuate during the reactor run, modifying the background noise level.[40,41]

In case an extensive environmental noise is expected, reducing the sidelobes and average sidelobes, and increasing SLSR is highly recommended. For designing a single FBG temperature sensor with very low sidelobe strength, average sidelobes, very high SLSR, high reflectivity, and narrow FWHM, Nuttall and New apodization functions would be the optimum choice for apodizations under discussion. Nuttall apodized FBG with length of 19000 μm and $\Delta n_{ac} = 4 \times 10^{-4}$ will have high reflectivity of 97.97%, narrow FWHM with 0.2135, very low sidelobe strength = −89.71 dB, average sidelobe = −90.79 dB, and very high SLSR of 89.62 dB. New apodized FBG with length of 8000 μm and $\Delta n_{ac} = 4 \times 10^{-4}$ will have high reflectivity of 74.6%, narrow FWHM with 0.255, very low sidelobe strength = −57.2 dB, average sidelobe = −60.4 dB, and high SLSR of 56 dB (*as marked with single underlined values in* Table II).

V. APODIZATION CHOICE FOR QUASI-DISTRIBUTED TEMPERATURE SENSING SYSTEM

For FBG based temperature sensor used in quasi-distributed sensing system, with the essential need of high adjacent channels isolation, efficient use of bandwidth, high roll-off rate, and large number of temperature sensors in the optical source wavelength range, it is necessary to have a smart choice of apodization profile, which has special characteristics to match these needs

To fulfill these needs for an array of FBGs, eliminating the sidelobes is certainly of much greater importance than in the single sensor's case because of the bad influence that sidelobes might have in determining the center frequency of the FBGs.[40] FBG has better resolution with narrower bandwidth, which is more preferable in practice because it requires smaller wavelength tunable range, and then can achieve higher measurement speed.[42] For quasi-distributed temperature sensing system (for free noise operation), results show that Barthann apodization function is the most suitable profiles that fulfill previous requirements.

Barthann apodization profile with length of 10000 μm and $\Delta n_{ac} = 2 \times 10^{-4}$ is a candidate. It provides a good reflectivity of 55%, narrow FWHM of 0.152 nm, low SL strength of −37.2 dB, low average sidelobe of −37.6 dB, high SLSR of 35 dB, and finally a very high sidelobe asymptotic decay of about 40 dB/nm, which will affect (enhance) the isolation between adjacent sensors. (*As marked with double underlined-values in* Table II)

It is not only the absolute reflectivity of the FBG that is important to have good detection of an FBG, but it is rather the SNR with which the FBG is measured that matters.[43] Noise is a so important factor that affects the FBG spectrum accuracy in obtaining the demodulated FBG information properly in case the intensity of the noise is relatively high. The good SNR is the premise of accurate wavelength demodulation.[44]

In remote temperature sensing systems, higher SNR permits for longer remote sensing distances, and works against the extensive noisy environments (RL is an example), very high SLSR is indeed needed. New apodization function is the optimum choice in this situation. New apodization profile with a length of 10000 μm and $\Delta n_{ac} = 2.5 \times 10^{-4}$ is a candidate. It provides reflectivity of 59.5%, good roll-off rate of about 18 dB/nm (low asymptotic decay can be neglected to some extend in case of very low sidelobes), and a high mainlobe slope of 86.7 dB/nm. New apodization function achieves narrow FWHM of 0.1775 nm (less than 25 GHZ), very low sidelobe strength of −60.1 dB, a very low sidelobe average level of −63.6 dB, and finally a high SLSR of 57.7 dB (*as marked with double underlined values in* Table II). These values are recommended for quasi-distributed temperature sensing systems and are different from those recommended for the single FBG temperature sensor, especially in noisy environments. In addition, the New apodization function is preferred in DWDM quasi-distributed temperature sensing system to avoid the undesired influence of sidelobes on the adjacent channels.

Fig. 10(a), shows the reflectivity spectrum for a five quasi-distributed FBG temperature sensing system with only Nuttall and Gaussian apodized FBG, as an example for the

Wavelengths with channel spacing of 2 nm and FWHM of 25 GHZ are recommended to be used according to the official ITU-T C-band grid (1546.12, 1548.11, 1550.12, 1552.12 and 1554.13 nm). Fig. 10(b) and 10(c), shows the corresponding five quasi-distributed FBG-based temperature sensors index profiles for Nuttall and Gaussian respectively, using the previously mentioned optimum design parameters.

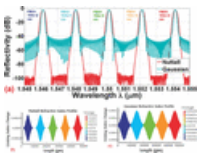

FIG. 10. (a) Five FBG temperature sensors reflectivity spectrum (Nuttall and Gaussian apodized), (b) the five quasi-distributed FBG-based Nuttall- apodized temperature sensors refractive index profiles (L = 10000 μm, $\Delta n_{ac} = 2.6 \times 10^{-4}$), (c) the five quasi-distributed FBG-based Gaussian- apodized temperature sensors refractive index profiles(L = 10000 μm, $\Delta n_{ac} = 2 \times 10^{-4}$).

A. Effect of roll-off rate and including unapodized FBG with other apodized FBG

In this section, the effect of designing a quasi-distributed sensing system containing an unapodized FBG-based temperature sensor among apodized sensors is discussed. The goal is to evaluate the effect of including a relatively high sidelobe, low asymptotic decay (low roll-off rate), and low SLSR apodization (uniform FBG in this case) on a quasi-distributed sensing system. This provides an assessment for the performance of combining more than one type of apodization profiles in the same sensing system, and to which extent the apodization functions pattern get affected.

Fig. 11(a)–11(e) shows the reflectivity patterns of five apodized FBGs, Gaussian, Hamming, Barthann, New, and Nuttall apodization functions respectively, with two nm channel spacing. Black pattern represents the spectrum when the apodized FBG3 is replaced with an unapodized one. FBG3 is a uniform FBG based temperature sensor and the others (FBG1, FBG2, FBG4, and FBG5) are apodized. Because of the uniform FBG high sidelobes and low roll-off rate, and the low SLSR, the apodized sensors reflectivity patterns (for wide range in the wavelength domain) are greatly affected (Black Spectrum). FBG1, FBG2, FBG4, and FBG5

wastes the apodization advantages.

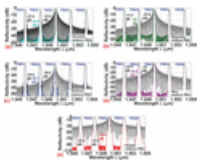

FIG. 11. Effect of an unapodized FBG-based temperature sensor on (a) four Gaussian apodized FBG sensor (b) four Hamming apodized FBG sensor (c) four Barthann apodized FBG sensor (d) four New function apodized FBG sensor (e) four Nuttall apodized FBG sensor.

PPT | High-resolution

Table IV summarizes Fig. 11(a)–11(e) results. The unapodized sensor does not affect the Barthann apodization function as much as other sensors for the adjacent and non-adjacent sensor SL. For the adjacent sensor SL strength, the Barthann is better than others are, whereas for the non-adjacent sensor SL, Barthann and Nuttall apodization function are almost the same and better than other apodization functions.

Table IV.

Effect of roll-off rate and unapodized FBG.

	Before Adding an unapodized FBG	After Adding an unapodized FBG	
	Max. SL (dB)	Max. SL (dB) (adjacent)	Max. SL (dB) (non-adjacent)
Gaussian	−39.6	−23.5	−27.6
Hamming	−51	−23.8	−31.5
Barthann	−40.1	−39.38	−36.8

Before Adding an unapodized FBG
After Adding an unapodized FBG
Max. SL (dB)
Max. SL (dB) (non-
Max. SL (dB)

PDF

New	−66.5	−23	−28.9
Nuttall	−98.8	−24.6	−36.5

This example shows the importance of the roll-off rate and its effect on whole system performance. A conclusion may be obtained by suggesting that, the quasi-distributed sensing system should not have a high SL, low SLSR, and low roll-off rate apodized sensor among other apodized sensors.

B. Effect of temperature on apodized FBG sensors and a linearity check

This section discusses and demonstrates FBG sensors with different apodization profiles influence on adjacent channel isolation in DWDM systems. Investigation of high performance FBG apodization profiles is groundwork for realization of high performance FBG-based quasi-distributed sensing systems with guaranteed high adjacent channels isolation.

Fig. 12 shows the effect of temperature on FBG2 (@ 1548.11 nm) as an example. The goal of this example is to predict the maximum allowable temperature that conserves 0.4 nm spacing between adjacent channels (suitable for DWDM – ITU standard) and then measures the corresponding isolation.

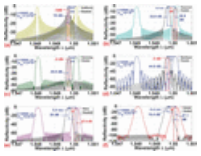

FIG. 12. Isolation and Temperature effect on FBG2 with $\Delta T = 117.3°C$. (a) Uniform (b) Gaussian apodization function (c) Hamming apodization function (d) Barthann apodization function (e) the New apodization function (f) Nuttall apodization function.

corresponding $\Delta\lambda_b$ (red shift) toward FBG3 (@ 1550.12 nm) is observed and depicted (according to the mathematical model sec. II eqn. (4)). A temperature difference $\Delta T = 117.3°C$ is obtained as the maximum allowable temperature range that makes FBG2 reflectivity peak at 0.4 nm spacing from FBG3 reflectivity peak as shown in Fig. 12.

The isolation between adjacent channels at $\Delta T = 117.3°C$ and channel spacing of 0.4 nm is determined. As we can see, the worst isolation shown is the FBG uniform apodization profile. This is mainly because of the great undesirable sidelobes bad influence on channels isolation. A high isolation is observed for the Barthann apodized sensor, this high isolation is enough to make FBG2 (with $\Delta T = 117.3°C$) and FBG3 reflectivity peaks highly distinguishable from each other at the optical detector side. To guarantee high channel isolation and therefore realize high performance quasi-distributed sensing systems, FBG sensors must be used with apodization functions that have narrow FWHM and low sidelobes. Uniform FBG profile showed the worst performance which result in whole system degradation (as shown in sec. V A, Fig. 11) because of the bad influence of high sidelobes on the channels isolation, whereas Gaussian, Hamming, Barthann, Nuttall, and the New apodization profiles show remarkable performance especially the Barthann profile.

1. Comparing with experimental results

Fig. 13 discusses the linearity issue for the discussed apodized FBG temperature sensor and highlights the relation between temperature and the corresponding wavelength.

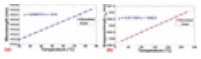

FIG. 13. Measured wavelength shift of the FBG sensors (a) A simulated temperature-wavelength relation of FBG at 1312 nm (b) simulated wavelength shift of the FBG sensor at 1548.61 nm.

Liu *et al* in Fig. 2,[45] made an experiment for a 3 mm length FBG at a central wavelength of 1312 nm. The bare FBG heated every 5 °C from $20°C$ to $80°C$. The fitting curve shows a linear relation between the temperature and the shifted wavelength as depicted. A sensitivity of $8.64 pm/°C$ is obtained. Fig. 13(a) is the simulated curve for that experiment at a wavelength of 1312 nm with a Gaussian apodization profile. A sensitivity of $9.47 pm/°C$ is obtained, and it matches what is obtained experimentally

Tam *et al*[46] made an experiment that shows the thermal shift of the Bragg wavelength for the temperature sensor with a center wavelength of 1548.61 nm, fitted by linear equation. The sensor is heated from 20 °C to 220°*C*. Red shift (wavelength increase) is observed with the increase of the FBG temperature. A temperature sensitivity of 11.8 pm/°C is obtained.[46] Fig. 13(b) is the simulated result for that experiment at a wavelength of 1548.61 nm. The simulation is done with Gaussian apodization profile and it shows a sensitivity of 11.18 *pm/°C* that agrees with the result obtained experimentally.

VI. CONCLUSION

In this work, different characteristics of FBG with various grating lengths (L) and refractive index (Δn_{ac}) change are studied. The quantitative analysis on maximum reflectivity, FWHM, average sidelobe, SLSR, sidelobe strength reduction, asymptotic decay level and roll-off rate is performed under new and different apodization profiles. Remarkable suppression of sidelobes and sidelobe average level, in the reflectivity pattern, for the Nuttall and Barthann apodization profiles on the expense of reduced reflected power is observed. The experimental results for the Gaussian apodization profile matches the simulated results.

For optimum single FBG-based temperature sensor performance, the Nuttall and the New apodization profiles achieve an outstanding performance. The Nuttall apodization profile achieves a high reflectivity of 97.97%, a narrow FWHM of 0.2135 nm, a very low sidelobe-strength of −89.71 dB, a very low sidelobe average of −90.79 dB, and finally a very high SLSR of 89.62 dB. The New apodization function extends its advantages and provides optimum results for quasi-distributed FBG-based temperature sensing systems. The Barthann apodization function also shows a remarkable performance in the quasi-distributed sensing systems.

A study on five apodized FBG-based temperature sensors in a quasi-distributed is analyzed and depicted. A simulation shows the bad influence of replacing the third apodized FBG (FBG3) with an unapodized FBG sensor.

With high sidelobe suppression, narrow FWHM, and high mainlobe slope, channels will be nearer together due to the negligible effect of sidelobes on the adjacent sensors reflectivity peaks, which leads to a higher possible capacity.

A study on isolation between adjacent sensors is performed. Barthann and Hamming apodizations show high isolation between adjacent sensors, which is necessary in quasi-distributed sensing systems. To guarantee high channel isolation and therefore realize high

apodization functions that have narrow FWHM, low sidelobes, and high slope.

A linear relation between temperature and the wavelength shift is observed experimentally and matched with the simulation results.

ACKNOWLEDGMENTS

The author thanks Eng. A. H. Ali Eldin for his help and information, Eng. Tamer F. Ismail for providing language help, Eng. Ashraf S. Helmy for his advice, and Mrs. Noha M. Hussein for her help and writing assistance.

REFERENCES

1. H. J. Dutton, Understanding optical communications. (Prentice Hall PTR, 1998). Google Scholar

2. V. Mizrahi, Components and devices for optical communications based on UV-written-fiber phase gratings presented at the Optical Fiber Communication Conference, 1993. Google Scholar, Crossref

3. J. Zhao, An object-oriented simulation program for fibre Bragg gratings, Rand Afrikaans University, 2001. Google Scholar

4. Y. Zhan, S. Xue, Q. Yang, S. Xiang, H. He, and R. Zhu, "A novel fiber Bragg grating high-temperature sensor Optik," International Journal for Light and Electron Optics **119**(11), 535–539 (2008). https://doi.org/10.1016/j.ijleo.2007.02.010 , Google Scholar, Crossref

5. J. Kou, S.-j. Qiu, F. Xu, and Y.-q. Lu, "Demonstration of a compact temperature sensor based on first-order Bragg grating in a tapered fiber probe," Opt. Express **19**(19), 18452–18457 (2011). https://doi.org/10.1364/OE.19.018452 , Google Scholar, Crossref

6. N. Liu, Y. Li, Y. Wang, H. Wang, W. Liang, and P. Lu, "Bending insensitive sensors for strain and temperature measurements with Bragg gratings in Bragg fibers," Opt. Express **19**(15), 13880–13891 (2011). https://doi.org/10.1364/OE.19.013880 , Google Scholar

7. H. Li, H. Yang, E. Li, Z. Liu, and K. Wei, *Wearable sensors in intelligent clothing for measuring human body temperature based on optical fiber Bragg grating* (2012). Google Scholar

8. M. Comanici, L. Chen, P. Kung, and L. Wang, Measurement of dynamic strain using a fiber Bragg grating-based laser sensor system presented at the Information Photonics (IP), 2011 ICO International Conference on, 2011. Google Scholar, Crossref

9. F. Urban, J. Kadlec, R. Vlach, and R. Kuchta, "Design of a pressure sensor based on optical fiber Bragg grating lateral deformation," Sensors **10**(12), 11212–11225 (2010). https://doi.org/10.3390/s101211212 , Google Scholar, Crossref

10. Q. Jiang and D. Hu, "Microdisplacement sensor based on tilted fiber Bragg grating transversal load effect," Sensors Journal, IEEE **11**(9), 1776–1779 (2011). https://doi.org/10.1109/JSEN.2010.2103399 , Google Scholar, Crossref

11. B. Gu, M. Yin, A. P. Zhang, J. Qian, and S. He, "Optical fiber relative humidity sensor based on FBG incorporated thin-core fiber modal interferometer," Optics express **19**(5), 4140–4146 (2011). https://doi.org/10.1364/OE.19.004140 , Google Scholar, Crossref

12. A. Stefani, W. Yuan, S. Andresen, and O. Bang, Polymer optical fiber bragg grating sensors: measuring acceleration presented at the Optical Fibre Technology (ACOFT), 2010 35th Australian Conference on, 2010. Google Scholar

13. C. Ambrosino, P. Capoluongo, S. Campopiano, A. Cutolo, M. Giordano, D. Davino, C. Visone, and A. Cusano, "Fiber bragg grating and magnetic shape memory alloy: Novel high-sensitivity magnetic Sensor," Sensors Journal, IEEE **7**(2), 228–229 (2007). https://doi.org/10.1109/JSEN.2006.886905 , Google Scholar, Crossref

14. K. Reck, E. V. Thomsen, and O. Hansen, "MEMS Bragg grating force sensor," Optics express **19**(20), 19190–19198 (2011). https://doi.org/10.1364/OE.19.019190 , Google Scholar, Crossref

"Two dimensional polymer-embedded quasi-distributed FBG pressure sensor for biomedical applications," Opt. Express **18**(1), 179–186 (2010). https://doi.org/10.1364/OE.18.000179 , Google Scholar, Crossref

16. M. Moccia, M. Pisco, A. Cutolo, V. Galdi, P. Bevilacqua, and A. Cusano, "Opto-acoustic behavior of coated fiber Bragg gratings," Optics express **19**(20), 18842–18860 (2011). https://doi.org/10.1364/OE.19.018842 , Google Scholar, Crossref

17. W. Ecke and K. Schroeder, Fiber Bragg grating optochemical sensor basing on evanescent-field interaction with surface plasmon waves presented at the The 16th International Symposium on: Smart Structures and Materials & Nondestructive Evaluation and Health Monitoring, 2009. Google Scholar, Crossref

18. H. Venghaus, "Wavelength filters in fibre optics," Wavelength Filters in Fibre Optics **1** (2006). https://doi.org/10.1007/3-540-31770-8 , Google Scholar, Crossref

19. R. W. Fallon, Fibre Bragg grating strain sensors, Aston University, 2000. Google Scholar

20. G. J. de Villiers, J. Treurnicht, and R. T. Dobson, "In-core high temperature measurement using fiber-Bragg gratings for nuclear reactors," Applied Thermal Engineering **38**, 143–150 (2012). https://doi.org/10.1016/j.applthermaleng.2012.01.024 , Google Scholar, Crossref

21. G. C. Righini, An introduction to optoelectronic sensors. (World Scientific, 2009). Google Scholar, Crossref

22. V. M. Sunita P. Ugale, *Optimization of Apodized Fiber Bragg Grating for Sensing Applications* IJCA Special Issue on Electronics, Information and Communication Engineering ICEICE(3) (December 2011). Google Scholar

23. *Dense Wavelength-division Multiplexing* http://www.fiber-optics.info/articles/dense_wavelength-division_multiplexing (2013). Google Scholar

Google Scholar

25. *Jphotonics Copal™ Series FBG Thermometer_Jphotonics, Inc. Fiber Bragg Grating, FBG interrogator, FBG sensors, Distributed Temperature Sensing (DTS)* http://www.jphotonics.com/product.asp?id=717 (2013). Google Scholar

26. A. Cusano, P. Capoluongo, A. Cutolo, and M. Giordano, "Chirped fiber-Bragg grating as self-temperature referenced strain sensor in nonisothermal thermoset processing," Sensors Journal, IEEE **6**(1), 111–117 (2006). https://doi.org/10.1109/JSEN.2005.856546 , Google Scholar, Crossref

27. S. A. Khan and M. Islam, Chromatic dispersion compensation using linearly chirped apodized fiber Bragg grating presented at the Electrical and Computer Engineering (ICECE), 2010 International Conference on, 2010. Google Scholar, Crossref

28. O. Mahran, T. A. Hamdallah, M. H. Aly, and A. E. El-Samahy, "Reflectivity of Nonlinear Apodized Chirped Fiber Bragg Grating Under Water," Journal of Applied Sciences Research **5**(10), 1604–1610 (2009). Google Scholar

29. D. L. Aybatov, R. R. Kiyamova, O. G. Morozov, and E. V. Suhorukova, *Distributed temperature fiber Bragg grating sensor* presented at the Optical Technologies for Telecommunications 2008, 2008. Google Scholar

30. M. Ferchichi, M. Najjar, and H. Rezig, *Design of temperature-strain tunable UDWDM, DWDM, WDM FBG filter for Passive Optical Network Access* presented at the Mediterranean Winter, 2008. ICTON-MW 2008. 2nd ICTON, 2008. Google Scholar

31. S. P. Ugale and V. Mishra, Optimization of fiber Bragg grating length for maximum reflectivity presented at the Communications and Signal Processing (ICCSP), 2011 International Conference on, 2011. Google Scholar, Crossref

32. Ravijot Kaur and M. Singh Bhamrah, "Effect of Grating length on Reflection Spectra of Uniform Fiber Bragg Gratings," International Journal of Information and Telecommunication Technology **3**(2) (2011). Google Scholar

33. I. Yulianti, S. Idrus, and A. Al-Hetar, Simulation of apodization profiles performances for unchirped fiber Bragg gratings presented at the Photonics (ICP), 2010 International Conference on, 2010. Google Scholar, Crossref

34. S. Ugale and V. Mishra, "Fiber Bragg Grating Modeling, Characterization and Optimization with different index profiles," International Journal of Engineering Science and Technology **2**(9), 4463–4468 (2010). Google Scholar

35. M. Bass and E. W. Van Stryland, Fiber Optics Handbook: Fiber, Devices, and Systems for Optical Communications. (McGraw-Hill New York, 2002). Google Scholar

36. X. Li, Q. Sun, P. Shum, N. Q. Nam, T. Cheng, and D. Liu, *A multi-point temperature warning sensor system with different thresholds using a multi-channel reference FBG* presented at the Asia Pacific Optical Communications, 2007. Google Scholar

37. R. P. Haaksman, Design of a fibre optic acoustic sensor array: sensitivity and noise properties, University of Southampton, 2002. Google Scholar

38. Y. Zhao, R. Hou, and C. Zhou, "Writing wide bandwidth nonchirped fiber Bragg gratings with high sidelobe suppression ratio by linearly scaling apodization," Optical Engineering **49**(8), 085001–085001 (2010). https://doi.org/10.1117/1.3475947 , Google Scholar, Crossref

39. *Advanced Optics Solutions* http://www.aos-fiber.com (September, 2013). Google Scholar

40. G. J. De Villiers, In-core temperature measurement for the PBMR using fibre-bragg gratings (University of Stellenbosch, Stellenbosch, 2009). Google Scholar

41. B. Brichard, M. Van Uffelen, A. F. Fernandez, F. Berghmans, M. Decréton, E. Hodgson, T. Shikama, T. Kakuta, A. Tomashuk, and K. Golant, "Round-robin evaluation of optical fibres for plasma diagnostics," Fusion engineering and design **56**, 917–921 (2001). https://doi.org/10.1016/S0920-3796(01)00418-5 , Google Scholar, Crossref

Bragg gratings interrogated by narrow linewidth tunable lasers," Optics express **19**(21), 20214–20223 (2011). https://doi.org/10.1364/OE.19.020214 , Google Scholar, Crossref

43. *FBGS - Draw Tower Gratings* http://www.fbgs.com (September, 2013). Google Scholar

44. D. Kong, J. Chang, P. Gong, Y. Liu, B. Sun, X. Liu, P. Wang, Z. Wang, W. Wang, and Y. Zhang, "Analysis and improvement of SNR in FBG sensing system," Photonic Sensors **2**(2), 148–157 (2012). https://doi.org/10.1007/s13320-012-0053-8 , Google Scholar, Crossref

45. M. Liu, E. Zhang, Z. Zhou, Y. Tan, and Y. Liu, "Measurement of Temperature Field for the Spindle of Machine Tool Based on Optical Fiber Bragg Grating Sensors," Advances in Mechanical Engineering 2013 (2013). Google Scholar

46. T. T. Tam, D. Q. Trung, T. A. Vu, L. H. Minh, and D. N. Chung, "Investigation of the embedded fiber bragg grating temperature sensor," VNU Journal of Science Mathematics-Physics **23**, 237–242 (2007). Google Scholar

General Information

ABOUT

CONTACT

HELP

PRIVACY POLICY

TERMS OF USE

FOLLOW AIP PUBLISHING:

Scitation

PDF